JCI The Journal of Clinical Investigation

SOD1 mutations disrupt redox-sensitive Rac regulation of NADPH oxidase in a familial ALS model

Maged M. Harraz, … , Christian Schöneich, John F. Engelhardt

J Clin Invest. 2008;118(2):659-670. https://doi.org/10.1172/JCI34060.

Research Article

Neurodegeneration in familial amyotrophic lateral sclerosis (ALS) is associated with enhanced redox stress caused by dominant mutations in superoxide dismutase–1 (SOD1). SOD1 is a cytosolic enzyme that facilitates the conversion of superoxide ($O_2^{\bullet-}$) to H_2O_2. Here we demonstrate that SOD1 is not just a catabolic enzyme, but can also directly regulate NADPH oxidase–dependent (Nox-dependent) $O_2^{\bullet-}$ production by binding Rac1 and inhibiting its GTPase activity. Oxidation of Rac1 by H_2O_2 uncoupled SOD1 binding in a reversible fashion, producing a self-regulating redox sensor for Nox-derived $O_2^{\bullet-}$ production. This process of redox-sensitive uncoupling of SOD1 from Rac1 was defective in SOD1 ALS mutants, leading to enhanced Rac1/Nox activation in transgenic mouse tissues and cell lines expressing ALS SOD1 mutants. Glial cell toxicity associated with expression of SOD1 mutants in culture was significantly attenuated by treatment with the Nox inhibitor apocynin. Treatment of ALS mice with apocynin also significantly increased their average life span. This redox sensor mechanism may explain the gain-of-function seen with certain SOD1 mutations associated with ALS and defines new therapeutic targets.

SOD1 mutations disrupt redox-sensitive Rac regulation of NADPH oxidase in a familial ALS model

Maged M. Harraz,[1] Jennifer J. Marden,[1] Weihong Zhou,[1] Yulong Zhang,[1] Aislinn Williams,[2] Victor S. Sharov,[3] Kathryn Nelson,[1] Meihui Luo,[1] Henry Paulson,[4] Christian Schöneich,[3] and John F. Engelhardt[1,5,6]

[1]Department of Anatomy and Cell Biology and [2]Medical Scientist Training Program and Graduate Program in Neuroscience, University of Iowa Carver College of Medicine, Iowa City, Iowa, USA. [3]Department of Pharmaceutical Chemistry, School of Pharmacy, The University of Kansas, Lawrence, Kansas, USA. [4]Department of Neurology, [5]Department of Internal Medicine, and [6]Center for Gene Therapy, University of Iowa Carver College of Medicine, Iowa City, Iowa, USA.

Neurodegeneration in familial amyotrophic lateral sclerosis (ALS) is associated with enhanced redox stress caused by dominant mutations in superoxide dismutase–1 (SOD1). SOD1 is a cytosolic enzyme that facilitates the conversion of superoxide ($O_2^{\bullet-}$) to H_2O_2. Here we demonstrate that SOD1 is not just a catabolic enzyme, but can also directly regulate NADPH oxidase–dependent (Nox-dependent) $O_2^{\bullet-}$ production by binding Rac1 and inhibiting its GTPase activity. Oxidation of Rac1 by H_2O_2 uncoupled SOD1 binding in a reversible fashion, producing a self-regulating redox sensor for Nox-derived $O_2^{\bullet-}$ production. This process of redox-sensitive uncoupling of SOD1 from Rac1 was defective in SOD1 ALS mutants, leading to enhanced Rac1/Nox activation in transgenic mouse tissues and cell lines expressing ALS SOD1 mutants. Glial cell toxicity associated with expression of SOD1 mutants in culture was significantly attenuated by treatment with the Nox inhibitor apocynin. Treatment of ALS mice with apocynin also significantly increased their average life span. This redox sensor mechanism may explain the gain-of-function seen with certain SOD1 mutations associated with ALS and defines new therapeutic targets.

Introduction

Superoxide dismutase–1 (SOD1) is a ubiquitously expressed cytosolic enzyme that facilitates the conversion of superoxide ($O_2^{\bullet-}$) to H_2O_2 (1). Inherited dominant mutations in *SOD1* lead to progressive motor neuron loss in the cerebral cortex, brain stem, and spinal cord in adult-onset amyotrophic lateral sclerosis (ALS) (2). Oxidative stress and inflammation are thought to play major roles in the pathogenesis of ALS, and several sources of ROS — including mitochondria, NADPH oxidase (Nox), and the SOD1 mutant itself — have been proposed to elevate redox stress in ALS (3–5). For example, studies in *SOD1*^{G93A} transgenic ALS mice have recently demonstrated that deletion of *Nox2*, and to a lesser extent *Nox1*, can significantly slow disease progression and improve survival of ALS mice (3, 5). Although these studies implicate multiple *Nox* genes in the pathology of ALS, it remains unclear whether enhanced Nox-dependent redox stress in ALS is a primary or secondary event of disease caused by mutant SOD1. Currently it is thought that enhanced Nox2-dependent redox stress in ALS is a secondary event associated with microgliosis during later stages of the inflammatory processes. Recent studies using controlled expression of mutant SOD1 in motor neurons and glia have also demonstrated that these 2 cell types contribute to different phases of ALS disease progression — motor neurons in early phases of disease onset and microglia in later phase disease progression (6). These findings implicate primary defects in microglial and neuronal functions as a consequence of mutant SOD1 expression.

Seven known Nox catalytic subunits exist: Nox1, Nox2^{gp91phox}, Nox3, Nox4, Nox5, Duox1, and Duox2 (7, 8). NADPH oxidases generate $O_2^{\bullet-}$ by transferring an electron from NADPH to molecular oxygen. The most widely characterized Nox is phagocytic gp91phox (Nox2), which is also expressed in microglia (3) and a variety of other nonphagocytic cell types. Rac1 is a central activator of Nox2 and Nox1, along with several other subunits that can act in a cell-specific fashion to promote Nox complex activation (p40phox, p47phox, p67phox, NoxO1, and NoxA1) (7, 8). Despite the finding that Nox2 contributes to inflammatory components of ALS disease (3, 5), the mechanism(s) by which mutations in SOD1 lead to dysregulation of $O_2^{\bullet-}$ production by Nox2 remain poorly understood.

In the present study, we investigated whether primary defects in Nox regulation are caused by ALS-associated mutations in SOD1. Our findings demonstrate that SOD1 controlled GTP hydrolysis by Rac1 through a redox-dependent interaction uncoupled by an H_2O_2-mediated modification to Rac1. In this context, when SOD1 was bound to Rac1 under reducing conditions, GTP hydrolysis by Rac1 was inhibited. However, in oxidizing conditions, SOD1 dissociated from Rac1 and no longer inhibited intrinsic GTP hydrolysis by Rac1. ALS mutant forms of SOD1 more strongly associated with Rac1 and were less sensitive to redox uncoupling. These SOD1/Rac1 interactions created a redox-dependent sensor for activation of Rac1-dependent NADPH oxidases and the production of $O_2^{\bullet-}$ by

Nonstandard abbreviations used: ALS, amyotrophic lateral sclerosis; DHE, dihydroethidium; DPI, diphenyleneiodonium chloride; Nox, NADPH oxidase; $O_2^{\bullet-}$, superoxide; PMDF, primary mouse dermal fibroblast; PMEF, primary mouse embryonic fibroblast; PPHB, potassium phosphate buffer; SOD1, superoxide dismutase–1; TLC, thin-layer chromatography; X/XO, xanthine/xanthine oxidase.

Conflict of interest: The authors have declared that no conflict of interest existed while scientific results were obtained for the present work. Following completion of the research presented in this article, a relationship with a company was formed to move findings to clinical trials. The authors have no equity in this company.

Citation for this article: *J. Clin. Invest.* **118**:659–670 (2008). doi:10.1172/JCI34060.

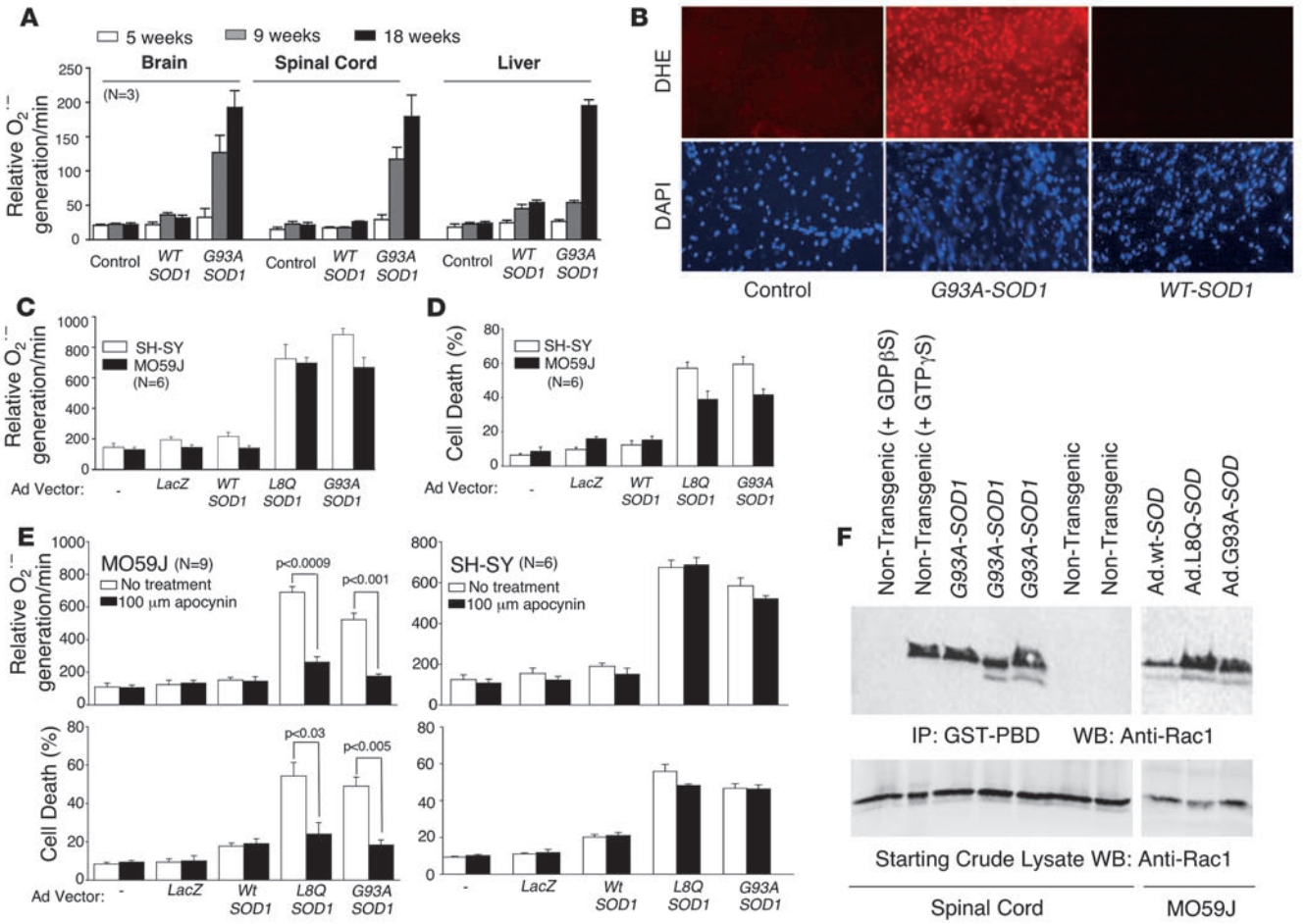

Figure 1

ALS-associated SOD1 mutations activate cellular Nox activity. (**A**) Rate of NADPH-dependent $O_2^{\bullet-}$ production by total endomembranes isolated from the brain, spinal cord, and liver of nontransgenic or transgenic mice overexpressing *SOD1*^{WT} or *SOD1*^{G93A} (mean ± SEM; n = 3 per group). (**B**) DHE fluorescent detection of $O_2^{\bullet-}$ in lumbar spinal cord sections from nontransgenic and transgenic mice overexpressing *SOD1*^{WT} or *SOD1*^{G93A}. DAPI staining shows cell nuclei in each section. (**C**) Rate of NADPH-dependent $O_2^{\bullet-}$ production in total endomembranes isolated from SH-SY (neuronal) or MO59J (glial) cells at 48 hours following infection with adenoviral vectors expressing LacZ, SOD1^{WT}, SOD1^{L8Q}, or SOD1^{G93A}. (**D**) Cell death was quantified in SH-SY and MO59J cells using trypan-blue exclusion at 72 hours after infection with the indicated adenoviral vectors. (**E**) Using conditions specified in **C** and **D**, the rate of NADPH-dependent $O_2^{\bullet-}$ production and cell death was assessed in the presence or absence of the Nox inhibitor apocynin (100 μM). Values are mean ± SEM (n = 6 per group). (**F**) Assessment of GTP-bound Rac1 (activated form) in spinal cord lysates from 2 nontransgenic or 3 *SOD1*^{G93A} transgenic mice (120 days old) and from MO59J cells overexpressing WT or mutant SOD1 proteins (at 36 hours after adenoviral infection). The 2 left lanes are controls for the Rac activation assay, in which nontransgenic spinal cord lysates were preincubated with the indicated non-hydrolysable guanine nucleotide analogs.

endomembranes. Importantly, this regulatory circuit was disrupted by familial ALS–associated mutations in SOD1. Hence, we propose a model by which SOD1 can directly regulate Nox activation by acting as a redox sensor for Rac1 inactivation. Such findings may help to explain the gain of function found in familial ALS SOD1 mutations associated with enhanced redox stress.

Results

ALS-associated SOD1 mutations activate cellular Nox activity. We hypothesized that ALS mutant SOD1, but not WT SOD1, directly dysregulates production of Nox-derived $O_2^{\bullet-}$. Indeed, analysis of transgenic mice overexpressing *SOD1*^{WT} or *SOD1*^{G93A} demonstrated that only the mutant form of SOD1 enhanced NADPH-dependent $O_2^{\bullet-}$ production in brain and spinal cord endomembranes and tissue (Figure 1, A and B), and that this was inhibited by the flavoprotein inhibitor diphenyleneiodonium chloride (DPI), but not the mitochondrial complex I inhibitor rotenone (Supplemental Figure 1, A and B; supplemental material available online with this article; doi:10.1172/JCI34060DS1). Interestingly, the liver, an organ that does not demonstrate notable pathology in ALS, also demonstrated similar SOD1 mutant–associated increases in Nox activity (Figure 1A).

To evaluate whether mutant SOD1 proteins enhance Nox activity directly in the absence of disease-associated inflammatory processes seen in vivo in ALS mice, we expressed WT, L8Q, and G93A forms of SOD1 in both MO59J glial cells and SH-SY neuronal cells using recombinant adenoviruses. Overexpression only of the mutant SOD1 proteins enhanced NADPH-dependent $O_2^{\bullet-}$ production in endomembranes from both glial and neuronal cell

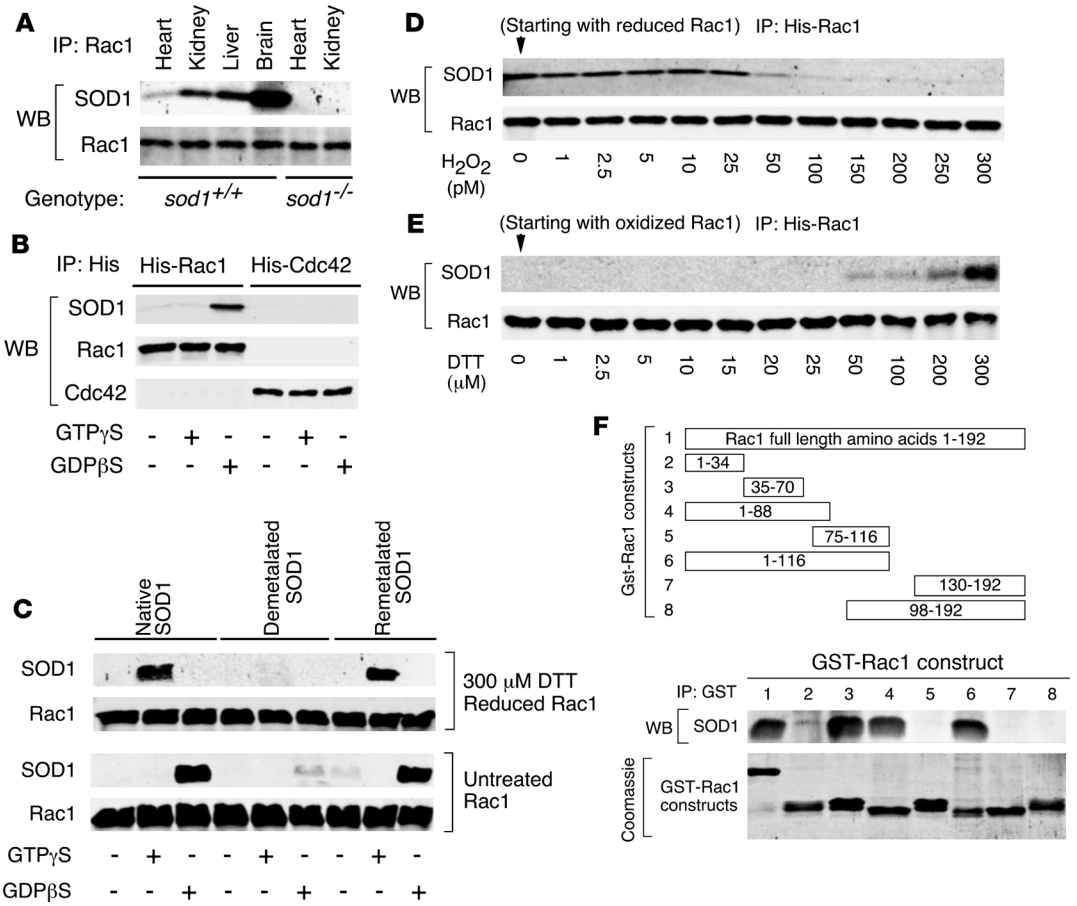

Figure 2

Rac1 binds to SOD1 in a redox-dependent manner. (**A**) Rac1 IP from heart, kidney, liver, and/or brain tissue of *SOD1*$^{+/+}$ or *SOD1*$^{-/-}$ mice followed by Western blotting (WB) for SOD1 and Rac1. (**B**) In vitro IP of purified His-tagged Rac1 and Cdc42 in the presence of purified bovine SOD1 followed by Western blot for SOD1, Rac1, and Cdc42. The His-tagged GTPases were preloaded with the indicated nucleotide analogs prior to incubation with SOD1. (**C**) In vitro IP of purified His-tagged Rac1 in the presence of purified native, demetalated, or remetalated bovine SOD1 followed by Western blot for SOD1 and Rac1. The His-tagged Rac1 was preloaded with the indicated nucleotide analogs prior to incubation with SOD1. Additionally, untreated His-tagged Rac1 and 300 μM DTT prereduced His-tagged Rac1 were used for in vitro pulldown assays with each of the 3 forms of SOD1. (**D**) His-tagged Rac1 was prereduced (300 μM DTT), loaded with GTPγS, and treated with the indicated concentrations of H_2O_2 before performing pulldown assays with SOD1. (**E**) The indicated concentrations of DTT were added to the 300 pM H_2O_2-treated His-tagged Rac1 sample in **D**, and pulldown assays were performed with SOD1. (**F**) Schematic of GST-Rac1 deletion mutants used to define the SOD1 binding domain and in vitro IP of various GST-tagged Rac1 deletion mutants in the presence of purified bovine SOD1. GST-Rac1 fusion construct numbers above correspond with lane numbers below. Top lanes are Western blot for SOD1 following IP of GST; bottom lanes are Coomassie-stained gel of the purified fusion peptides used for IP.

types (Figure 1C) and significantly increased cell death (Figure 1D). These findings implicate a gain of function in SOD1 mutants that leads to enhanced Nox activation and cellular injury. Apocynin, a known inhibitor of NADPH oxidases such as Nox2 (9), abrogated SOD1 mutant–facilitated NADPH-dependent $O_2^{\bullet-}$ production only in glial cells, with a corresponding increase in cell viability (Figure 1E). In contrast, apocynin did not inhibit NADPH-dependent $O_2^{\bullet-}$ production in SH-SY neuronal cells induced by mutant SOD1 expression, nor did it protect from associated cellular injury (Figure 1E). These findings suggest that dysregulated ROS production in SOD1 mutant–expressing neuronal cells likely occurs through a pathway distinct from that in glial cells.

Apocynin is thought to inhibit NADPH oxidases by interfering with recruitment of p47phox to the Nox complex (10). Three known Nox catalytic subunits have been shown to be regulated by p47phox in vitro (Nox1, Nox2, and Nox3) (7, 11) and these Nox isoforms are also regulated by the small GTPase Rac (8). However, thus far only Nox2 has been confirmed to be regulated by p47phox in vivo. To this end, we hypothesized that mutant SOD1 expression in apocynin-responsive MO59J glial cells enhances Rac1 activation. Indeed, both $SOD1^{G93A}$ and $SOD1^{L8Q}$ mutant proteins elevated Rac1-GTP levels in MO59J cells compared with overexpression of $SOD1^{WT}$, as determined by Pak1 pulldown assays (Figure 1F). More importantly, spinal cords from ALS transgenic mice overexpressing the $SOD1^{G93A}$ mutant demonstrated an even greater enhancement in Rac1-GTP levels (i.e., activated Rac1) compared with nontransgenic age-matched controls (Figure 1F). These findings of enhanced Rac1 activation by SOD1 mutant expression led us to hypothesize that SOD1 directly interacts with Rac1 and/or other Nox complex components to stabilize the activated form of

this complex. In support of this hypothesis are previous findings that SOD1 and Rac1 both recruit to Nox2-active early endosomes following cytokine stimulation (12).

Rac1 binds to SOD1 in a redox-dependent manner. To investigate potential binding partners for SOD1 that were associated with the Nox complex, we performed IP experiments for p47phox, p67phox, p22phox, and Rac1 — 4 regulators of the Nox2 complex — from brain tissue lysates followed by Western blotting for SOD1 and found that only Rac1 effectively pulled down SOD1 (Figure 2A and data not shown). To determine whether Rac1/SOD1 interactions occur in other tissue types, we conducted co-IP experiments from several mouse organs including brain, liver, kidney, and heart. Indeed, IP of Rac1 pulled down SOD1 from each of these organs in *SOD1*$^{+/+}$ mice, but not *SOD1*$^{-/-}$ mice (Figure 2A). The amount of SOD1 associated with Rac1 was noticeably highest in the brain and lowest in the heart. To test whether this interaction was direct, we used in vitro pulldown assays with purified proteins. Immobilized His-tagged Rac1 clearly associated with SOD1 when Rac1 was preloaded with GDPβS, but not when Rac1 was preloaded with GTPγS or in the absence of nucleotide (Figure 2B). In contrast, the related Rho GTPase Cdc42 did not associate with SOD1 (Figure 2B). These results suggested that the GDP-bound form of Rac1 associates with SOD1.

Given that Rac1 can regulate $O_2^{\bullet-}$ production through certain NADPH oxidases (13, 14) and that SOD1 dismutates $O_2^{\bullet-}$ to H_2O_2, we hypothesized that SOD1 enzymatic activity is fundamentally important for interactions with Rac1. Cu binding at the active site of SOD1 is necessary for its enzymatic activity, and a specific Cu chaperone is required for the loading of SOD1 with Cu in vivo (15). Using in vitro pulldown assays, we asked whether the interaction between Rac1 and SOD1 was redox regulated and whether the metal content of SOD1 affected this interaction. Interestingly, reduction of Rac1 with DTT switched the nucleotide preference required for binding to SOD1 (Figure 2C). Nonreduced bacterially expressed Rac1 most efficiently bound to SOD1 in the presence of GDPβS, as shown in Figure 2B. In contrast, reduced Rac1 bound to SOD1 when loaded with GTPγS but not GDPβS (Figure 2C). Furthermore, only metalated (i.e., native) and remetalated forms of SOD1 bound to Rac1, while demetalated (i.e., enzymatically inactive) SOD1 failed to bind Rac1 (Figure 2C and Supplemental Figure 2A). In contrast, neither reduced Cdc42-GTPγS nor Cdc42-GDPβS bound SOD1 (Supplemental Figure 2B). These findings demonstrate that SOD1 can indeed bind Rac1-GTP under reducing conditions and suggest that the redox state of Rac1 influences its affinity for SOD1 in GTP versus GDP bound states.

Intrigued by these results, we sought to directly test whether sequential reduction and oxidation of GTP-bound Rac1 cycles Rac1 into SOD1 bound and unbound states, respectively. To this end, we exposed Rac1 (reduced with DTT and preloaded with GTPγS) to different concentrations of H_2O_2 and evaluated its ability to associate with SOD1 after removing excess H_2O_2 and found that H_2O_2 concentrations as low as 50 pM caused a significant decrease in the binding affinity of Rac1 for SOD1 (Figure 2D). To exclude the possibility of H_2O_2-mediated irreversible damage to Rac1 protein, we repeated the same experiment adding back different concentrations of DTT to oxidized Rac1 exposed to 300 pM H_2O_2. Indeed, H_2O_2-mediated inhibition of Rac1/SOD1 binding was reversed by treatment of Rac1 with 50–300 μM DTT (Figure 2E). These in vitro association data demonstrate that Rac1/SOD1 binding is redox regulated and can cycle between bound and unbound states depending on the redox state of Rac1.

To determine the domain of Rac1 that associated with SOD1, we constructed GST-tagged deletion mutants of Rac1 (Figure 2F) and conducted in vitro pulldown assays. SOD1 most efficiently bound a region of Rac1 contained within amino acids 35–70 (Figure 2F). This region of Rac1 spans several domains important for nucleotide binding (i.e., switch I, G2, switch II, and G3 domains; Supplemental Figure 2C; refs. 16–18). Binding of SOD1 to this region on Rac1 is also consistent with the observed differences in binding between SOD1 and GTPγS- versus GDPβS-bound Rac1. Interestingly, Rac1 guanine-nucleotide exchange factor (GEF) Tiam1 binds to a region of Rac1 that spans the interacting domain with SOD1 (19). In addition, the switch regions on 2 related Rho GTPases, RhoA and Cdc42, are involved in binding to RhoGAP (20, 21). Therefore, we hypothesized that SOD1 influences Rac1 activity by acting as a GEF or GAP. However, SOD1 did not significantly affect GTP loading on Rac1 in vitro (Supplemental Figure 2D) and hence appeared not to act as a GEF.

SOD1 regulates Rac1/Nox2 activation, and this function is dysregulated in certain SOD1 ALS mutants. We next evaluated whether SOD1 serves as a GAP to stimulate GTP hydrolysis by Rac1. Such a hypothesis was consistent with elevated Rac1-GTP levels in mutant SOD1–expressing glial cells and spinal cord (Figure 1F). However, SOD1 significantly inhibited the GTPase activity of Rac1 and also prevented p29Rho-GAP from activating GTP hydrolysis by Rac1 (Figure 3A). However, *E. coli* SOD, a homolog of mammalian MnSOD/SOD2, did not alter Rac1 GTPase activity (Figure 3B), nor did it associate with Rac1 in vitro (data not shown). The ability of SOD1 to inhibit GTP hydrolysis was also specific for Rac1 and was not observed with the closely related small GTPase Cdc42 (Figure 3C). Furthermore, demetalated (i.e., enzymatically inactive) SOD1, which did not associate with Rac1 (Figure 2C), also did not inhibit Rac1 GTPase activity (Supplemental Figure 2E). Given that Rac1 has exceptionally high intrinsic GTPase activity (22), these findings are consistent with SOD1 acting to stabilize Rac1-GTP by inhibiting its GTPase activity.

Because the binding of Rac1 to SOD1 was controlled by the redox state of Rac1, we hypothesized that the ability of SOD1 to regulate Rac1 GTPase activity might also be redox regulated. To directly evaluate whether ROS alter the ability of SOD1 to inhibit GTP hydrolysis by Rac1, we performed GTPase assays in the presence of a xanthine/xanthine oxidase (X/XO) $O_2^{\bullet-}$ generating system. Given that Rac1 regulates $O_2^{\bullet-}$ production by certain NADPH oxidases, such a question was potentially relevant to processes that regulate ROS production in vivo. Interestingly, SOD1 lost its ability to inhibit GTP hydrolysis by Rac1 in the presence of this ROS-generating system (Figure 3D). However, the levels of ROS generated under our experimental conditions did not affect the intrinsic Rac1 GTPase activity in the absence of SOD1 (Figure 3D). IP of Rac1-GTPγS/SOD1 complexes using the GTPase assay conditions demonstrated that exposure to X/XO-derived ROS dissociated SOD1 from Rac1 (Figure 3E). These findings demonstrated that ROS alter the ability of SOD1 to regulate Rac1 GTPase activity by controlling physical interactions between these 2 proteins. These findings are consistent with the ability of H_2O_2 to disrupt SOD1/Rac1 interactions (Figure 2D).

Rac1 and Rac2 are well recognized for their ability to regulate cellular $O_2^{\bullet-}$ through its interactions with Nox1 and Nox2^{gp91phox} (7). Rac2 is a hematopoietic-specific protein and regulates Nox2^{gp91phox}

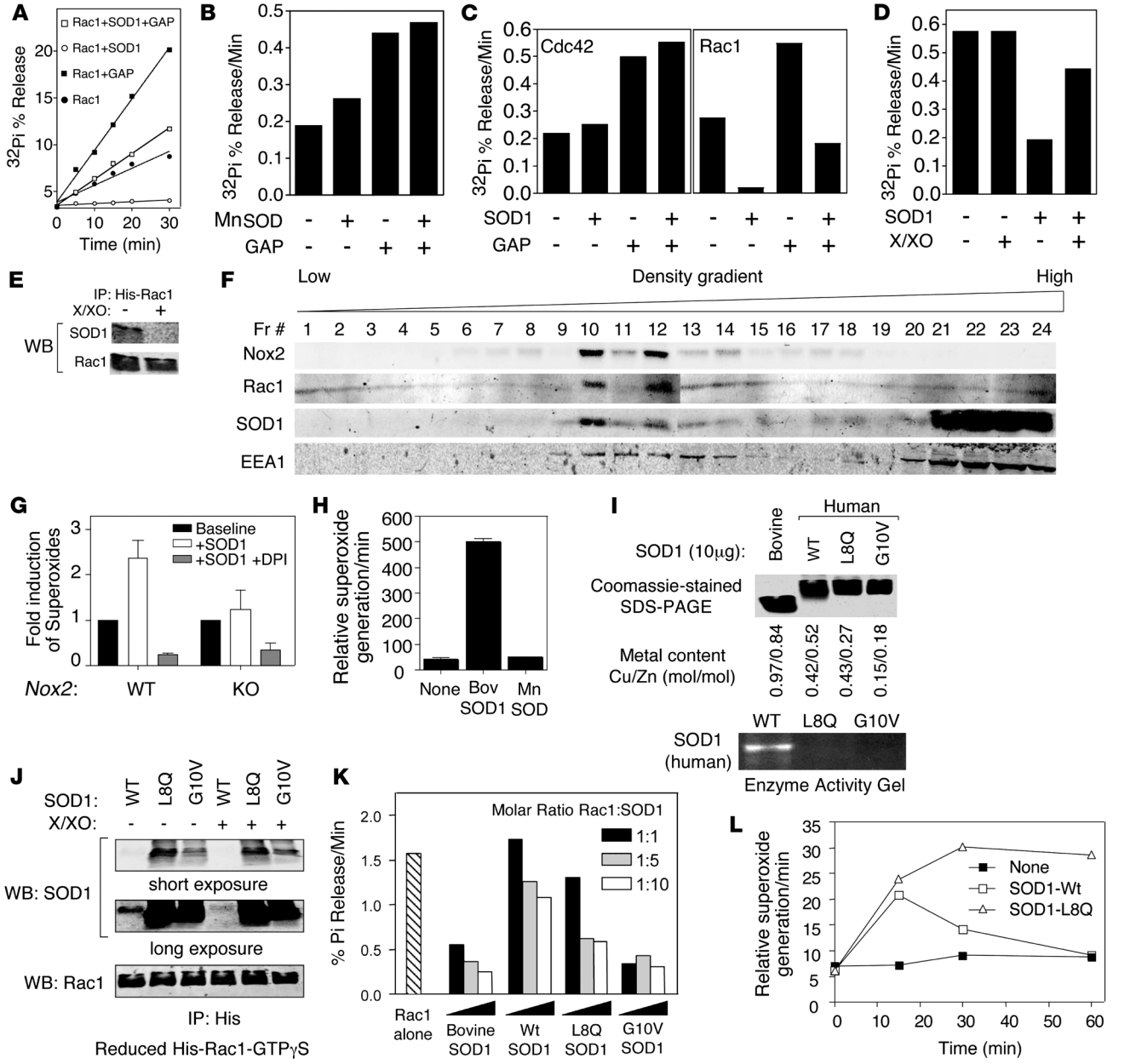

Figure 3

SOD1 activates Rac1 and Nox2, a function dysregulated in certain SOD1 ALS mutants. (**A** and **B**) Rac1 GTPase assays were performed in the presence or absence of purified (**A**) bovine SOD1 or (**B**) *E. coli* MnSOD and/or p29-GAP. His-tagged Rac1 was preloaded with γP^{32}-GTP, and aliquots of the reaction were analyzed at various time points by TLC for GTP hydrolysis by assessing percent ^{32}Pi released from Rac1. (**C**) GTPase assay for Rac1 and Cdc42 in the presence or absence of bovine SOD1 and/or p29-GAP. (**D**) Rac1 GTPase assay in the presence or absence of bovine SOD1 and/or X/XO (100 mU; final concentration 100 μM). (**E**) Pulldown assays of GTPγS-loaded His-tagged Rac1 in the presence of bovine SOD1 with or without 15-minute exposure to X/XO-derived ROS. Data are representative of at least 3 independent experiments. (**F**) Endosomes were isolated from PMDFs using Iodixanol density gradient fractionation, and fractions were characterized by Western blot for $Nox2^{gp91phox}$, Rac1, SOD1, and EEA1. (**G**) Lucigenin assays were used to assess the rate of NADPH-dependent $O_2^{\bullet-}$ production in fraction 10 vesicles from *Nox2* WT and KO PMDFs in the presence or absence of 2.5 μM bovine SOD1 and/or 10 μM DPI, a general Nox inhibitor ($n = 6$). (**H**) Vesicular fractions from PMEFs heterozygous for a gene disruption of mouse SOD1 were assessed for NADPH-dependent $O_2^{\bullet-}$ production in the presence or absence of exogenously added 2.5 μM bovine SOD1 or 2.5 μM *E. coli* MnSOD ($n = 3$). (**I**) Coomassie-stained SDS-PAGE of purified bacterially expressed human SOD1 proteins. Bovine SOD1 was used as a reference control and migrates faster than human SOD1 (12). The Cu/Zn content of each SOD1 protein is shown. SOD activity gel of the bacterial purified SOD1 proteins is shown at bottom. (**J**) In vitro IP of purified prereduced His-tagged Rac1-GTPγS in the presence of the indicated human SOD1 proteins. Rac1/SOD1 complexes were then divided into 2 parts; 1 half was treated with X/XO-derived ROS for 15 minutes at room temperature prior to IP of the His-tag. Following IP, Western blots for SOD1 and Rac1 were performed. Long and short exposures of the SOD1 blot are shown to demonstrate enhanced binding of each of the mutant forms of SOD1 to Rac1. (**K**) Rac1 GTPase assays were performed using native bovine SOD1 or the indicated bacterially expressed purified human SOD1 proteins. The molar ratio of Rac1/SOD1 is indicated. (**L**) Time course of NADPH-dependent $O_2^{\bullet-}$ generation by isolated PMEF endosomes in the presence or absence of 1 μM human $SOD1^{WT}$ or $SOD1^{L8Q}$.

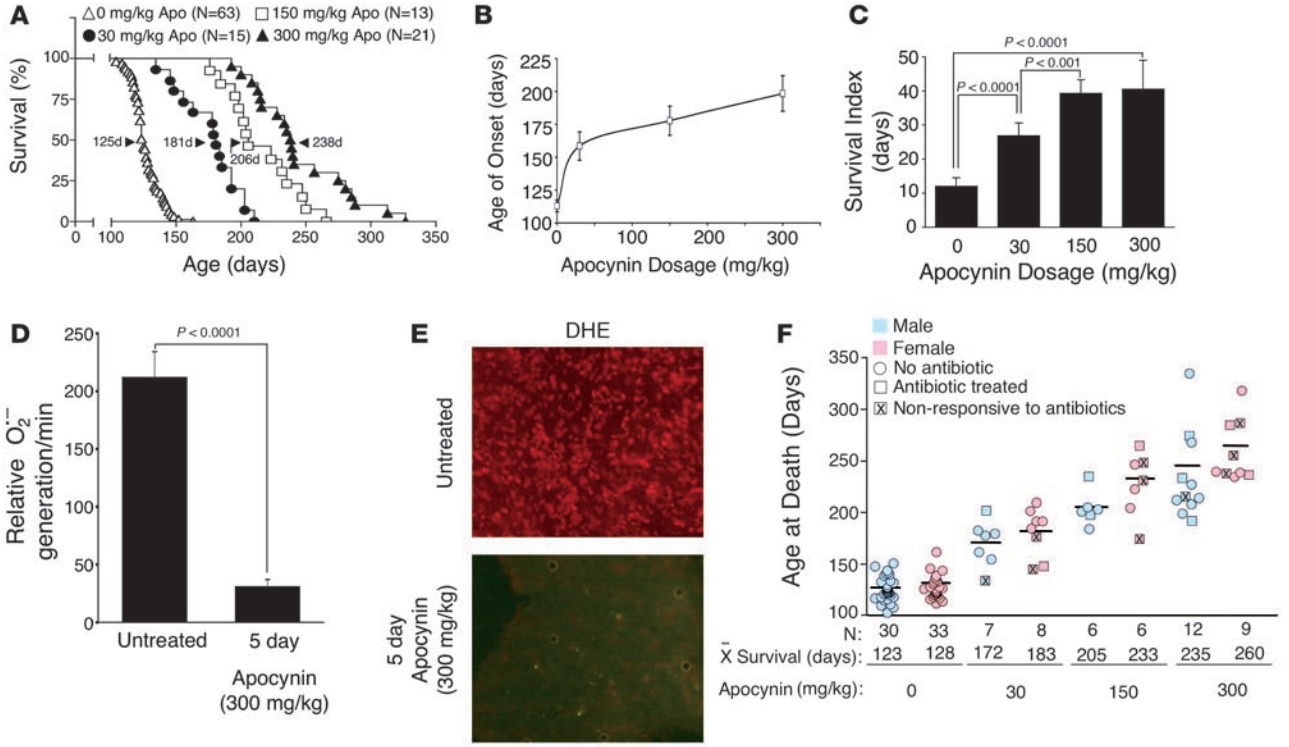

Figure 4

Treatment with the Nox inhibitor apocynin increases lifespan and slows disease progression in mice hemizygous for the *SOD1*^{G93A} transgene. (**A**) Kaplan-Meier survival curve for mice treated with indicated doses of apocynin in their water beginning at 14 days of age. *n* is shown along with median survival time (arrowhead) for each group. Survival differences were significant in all between-group comparisons (log-rank test). (**B**) Age of disease onset, as determined by a 10% weight loss from peak body weight, for the various doses of apocynin. (**C**) Dose affect of apocynin treatment on survival index, measured as time from disease onset (as determined by weight loss) until clinical death. (**D**) Rate of NADPH-dependent $O_2^{\bullet-}$ production in total endomembranes isolated from lumbar spinal cords of end-stage *SOD1*^{G93A} transgenic mice (~120 days of age) that were either untreated or treated with apocynin (300 mg/kg) in the drinking water for 5 days prior to harvesting spinal cords ($n = 5$ per group). (**E**) DHE fluorescence was assessed in lumbar spinal cord sections from 2 mice evaluated in **D**. (**F**) Survival data of male and female mice at the indicated apocynin dose. Mice treated for eye infections with antibiotics are marked as squares; those unsuccessfully treated that died from eye infections are marked by "X" within the square. Circles denote animals that never contracted eye infection. *n* and mean survival time is indicated for each group. Data in **B**–**D** are mean ± SEM.

in neutrophils (23). Rac1, on the other hand, is a ubiquitous protein that can regulate Nox1 (11, 24) as well as Nox2^{gp91phox} activity in human monocytes (25) and myeloid lineage cells such as microglia (26). These interactions have placed Rac1 central to a number of ROS-regulated cellular processes controlled by $O_2^{\bullet-}$ and/or H_2O_2, the dismutated product of $O_2^{\bullet-}$ (13, 27–30). Interestingly, we recently demonstrated that SOD1 is recruited to the surface of endosomes that produce lumenal Nox2-dependent $O_2^{\bullet-}$ following IL-1β activation (12). This led us to hypothesize that SOD1 activates Rac1/Nox2 complexes in the endosomal compartment to produce $O_2^{\bullet-}$ by inhibiting the GTPase activity of Rac1. To this end, we isolated unstimulated Nox2-containing endosomes from primary mouse dermal fibroblasts (PMDFs) and tested whether supplementing SOD1 would activate NADPH-dependent $O_2^{\bullet-}$ generation by this compartment. To confirm that endosomal $O_2^{\bullet-}$ was indeed derived from Nox2, we used PMDFs isolated from *Nox2*^{gp91phox} KO mice or WT control littermates. Iodixanol density gradient separation of vesicular fractions from WT heavy mitochondrial supernatant demonstrated 2 predominant peak fractions containing Nox2^{gp91phox}, Rac1, and SOD1 proteins (fractions 10 and 12) that overlapped with a small peak in NADPH-dependent $O_2^{\bullet-}$ production and the early endosomal marker EEA1 (Figure 3F). The addition of purified bovine SOD1 to these isolated endosomes led to a significant enhancement in their ability to produce NADPH-dependent $O_2^{\bullet-}$ (Figure 3G). This enhancement in endosomal $O_2^{\bullet-}$ was sensitive to DPI, a Nox inhibitor, and was not observed in *Nox2*^{gp91phox} KO PMDFs (Figure 3G), suggesting that the $O_2^{\bullet-}$ was indeed derived from Nox2. These results were reproduced in endosomes isolated from WT primary mouse embryonic fibroblasts (PMEFs), in which the production of NADPH-dependent $O_2^{\bullet-}$ was induced by the addition of bovine SOD1, but not *E. coli* SOD (Figure 3H), despite the equal capacity of both enzymes to dismutate $O_2^{\bullet-}$ (Supplemental Figure 3).

Our findings demonstrating that SOD1 can regulate Rac1/Nox2 activation in a redox-dependent fashion provided insights into SOD1 function. However, it remained unclear how ALS-associated mutations in SOD1 dysregulated Rac1 activation and Nox activity. To this end, we generated and purified WT human SOD1 and 2 human ALS mutant SOD1 proteins (L8Q and G10V) from bacteria as GST fusions and cleaved the GST prior to analysis (Figure 3I). Of note, generation of the SOD1^{G93A} GST fusion was unsuccessful, likely because of toxicity of this fusion in bac-

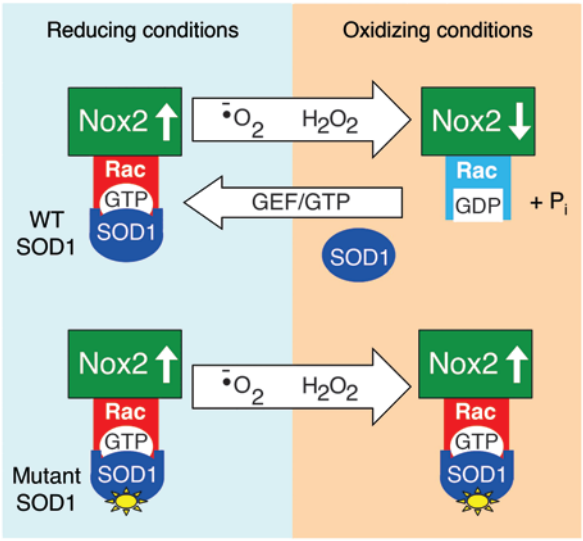

Figure 5

Redox-sensor model for SOD1-mediated regulation of Nox2 ROS production through Rac. Under reducing conditions SOD1 is bound to Rac-GTP and stabilizes Rac activation by inhibiting intrinsic and GAP-mediated GTP hydrolysis. Increased Rac-GTP levels lead to activation of Nox2 and production of $O_2^{\bullet -}$. $O_2^{\bullet -}$ generated by the Nox2 complex is converted to H_2O_2 by SOD1 or through spontaneous dismutation. As the local concentration of H_2O_2 rises, oxidation of Rac leads to the dissociation of SOD1. With SOD1 no longer bound to Rac-GTP, hydrolysis to Rac-GDP occurs more quickly, leading to inactivation of the Nox2 complex. SOD1 can then recycle to repeat the process as Rac/Nox2 is reactivated. Through this mechanism, we propose that SOD1 can sense the local concentration of ROS at sites of Rac/Nox2 complex activation and control the activity of the complex. In certain ALS mutants of SOD1, redox-dependent dissociation of SOD1 from Rac1 is impaired, leading to sustained activation of Rac1-GTP and higher levels of Nox2 activation.

teria. However, in contrast to previous studies demonstrating that $SOD1^{G93A}$ has normal enzymatic activity (31), $SOD1^{L8Q}$ and $SOD1^{G10V}$ proteins purified from *E. coli* lacked dismutase activity compared with $SOD1^{WT}$ prepared under the same conditions (Figure 3I). Interestingly, both human $SOD1^{L8Q}$ and $SOD1^{G10V}$ mutant proteins had enhanced ability to bind Rac1 when compared with human $SOD1^{WT}$ (Figure 3J). Unlike human $SOD1^{WT}$, binding of these SOD1 mutants to Rac1 was not disrupted by X/XO-derived ROS (Figure 3J), suggesting that the redox regulation of SOD1/Rac1 interactions is altered by L8Q and G10V mutations in SOD1. Importantly, human $SOD1^{L8Q}$ and $SOD1^{G10V}$ mutant proteins also demonstrated enhanced ability to inhibit Rac1-GTP hydrolysis compared with human $SOD1^{WT}$ (Figure 3K). Reduced metalation of bacterial-derived human $SOD1^{WT}$ led to decreased effectiveness for inhibiting Rac1-GTPase activity compared with purified bovine SOD1 (Figure 3I), which was likely the result of the reduced binding affinity to Rac1 shown in Figure 2C. However, the extent of metalation appeared to have less of an effect on the ability of bacterial-derived human mutant SOD1 proteins to bind Rac1 and inhibit GTPase activity.

Based on the above results, we hypothesized that certain ALS mutations in SOD1 might dysregulate Nox2 activation in the endosomal compartment by virtue of their more persistent and redox-insensitive activation of Rac1. To this end, we tested the time course of NADPH-dependent $O_2^{\bullet -}$ production by isolated endosomal fractions following the addition of human $SOD1^{WT}$ or $SOD1^{L8Q}$ proteins. As previously observed for bovine $SOD1^{WT}$ (Figure 3H), human $SOD1^{WT}$ activated the production of NADPH-dependent $O_2^{\bullet -}$ by isolated PMEF endosomes (Figure 3L). This activation in $O_2^{\bullet -}$ production peaked by 15 minutes and returned to baseline by 1 hour. Such transient activation was consistent with Nox-derived ROS inhibiting SOD1/Rac1 interactions and activating GTP hydrolysis by Rac1, leading to a self-regulated reduction in Nox activation. In contrast, adding $SOD1^{L8Q}$ to PMEF endosomes gave rise to persistent NADPH-dependent $O_2^{\bullet -}$ production, to 1 hour (Figure 3L). Collectively, these results suggest that the $SOD1^{L8Q}$ ALS mutant is dysregulated in its ability to activate Nox2 by virtue of altered redox-sensitive interactions with Rac1. Such findings are consistent with elevated Nox activity in spinal cords and brains of ALS mice.

Treatment with the Nox inhibitor apocynin increases lifespan and slows disease progression in ALS mice. Our finding that certain ALS-associated SOD1 mutations lead to primary defects in Nox activation suggests that inhibiting Nox activation may be therapeutically beneficial in ALS. Indeed, 2 recent studies have demonstrated that deletion of *Nox2* can enhance survival and delay disease onset in ALS mice (3, 5). In light of these findings, we tested whether apocynin administration in the drinking water from 2 weeks of age would prolong survival of hemizygous $SOD1^{G93A}$ mice. As shown in Figure 4A, apocynin treatment increased survival of ALS mice in a dose-dependent fashion. At the highest dose, 300 mg/kg, 50% survival times were increased from 125 to 238 days. Both the highest and lowest doses also significantly increased the number of motor neurons in the lumbar spinal cord at 120 days (Supplemental Figure 4, A and B), and there was a clear apocynin dose response in delaying age of disease onset. Treatment with apocynin also significantly increased the survival index of ALS mice (assessed as time to death from first signs of symptoms) using 2 confirmatory methods for onset of disease: weight loss (Figure 4, B and C) and gait (Supplemental Figure 4, C and D). Cumulatively, these findings demonstrated that long-term apocynin treatment significantly delayed disease progression in ALS mice. To confirm that apocynin treatment inhibited Nox activity in vivo, we also treated terminal-stage ALS mice for 5 days with apocynin in the water and evaluated Nox activity and ROS production in the spinal cord by lucigenin and dihydroethidium (DHE) assays, respectively. These studies demonstrated that apocynin treatment effectively inhibited NADPH-dependent $O_2^{\bullet -}$ production in vivo (Figure 4, D and E) at later stages of disease associated with microgliosis and increased Nox2 expression (3). The cellular level of increased DHE staining in the spinal cord also suggests that multiple cell types in addition to microglia may have enhanced redox stress. This notion is supported by the fact that multiple *Nox* genes (i.e., Nox1 and Nox2) have been shown to influence progression of disease in $SOD1^{G93A}$ transgenic mice (5).

One unexpected finding was that ALS mice with prolonged survival developed eye infections that, if left untreated, led to rapid death without the normal course of motor abnormalities. This was similarly observed in ALS mice on the *Nox2*-deficient background (5). Treatment of these eye infections with systemic antibiotics led to resolution in approximately 50% of cases (Figure 4F). Importantly, treatment of ALS mice with antibiotics did not increase survival in the absence of apocynin, and non-ALS mice treated with apocynin did not develop eye disease (data not shown).

Discussion

Our findings demonstrate that SOD1, an enzyme that ubiquitously directs the conversion of $O_2^{\bullet-}$ to H_2O_2 in cells, has the ability to control Rac1/Nox2 activation through redox-dependent physical interactions with Rac1. Based on our findings, we propose a redox sensor model by which SOD1 can regulate Nox2-dependent $O_2^{\bullet-}$ production through its ROS-sensitive control of Rac-GTP hydrolysis (Figure 5). Upon stimulation, activated Rac-GTP is recruited to the assembling membrane-associated Nox2 complex along with SOD1. Under the reducing conditions of the cytoplasm, SOD1 efficiently binds to Rac-GTP and inhibits intrinsic and/or GAP-facilitated GTPase activity, thereby maintaining Rac in the active state and consequently increasing the production of Nox2-derived $O_2^{\bullet-}$. Local accumulation of H_2O_2, by either spontaneous or SOD1-facilitated dismutation of $O_2^{\bullet-}$, leads to the dissociation of SOD1 from Rac-GTP and inactivation of Rac through GTP hydrolysis. Since Rac-GDP cannot support Nox2 activation, this event leads to inactivation of the Nox2 complex and reduction in ROS production. It is this redox-sensitive uncoupling of SOD1 from Rac that appears to be dysfunctional in certain ALS mutants of SOD1, leading to hyperactivation of Nox-derived $O_2^{\bullet-}$ by endomembranes.

The finding that SOD1 functions to regulate Rac1-dependent $O_2^{\bullet-}$ production by NADPH oxidases in a redox-dependent fashion has important implications for ALS and the development of targeted antioxidant therapies such as apocynin. Several antioxidant therapies directed at clearance of ROS have been previously evaluated in clinical trials and case studies for ALS (32–34). However, these studies have failed to enhance survival. The therapeutic effect of long-term apocynin administration to *SOD1*^{G93A} transgenic mice resembled or exceeded that of *Nox2* or *Nox1* deletion in the same ALS mouse model (5). The robust therapeutic effect of apocynin in preventing progression of ALS in this model suggests that inhibiting ROS production, as opposed to scavenging ROS, may be significantly more protective in ALS. The ability of picomolar quantities of H_2O_2 to liberate SOD1 from Rac-GTP and allow for GTP hydrolysis to occur suggests that the mechanism of in vivo regulation of Nox may be exquisitely sensitive to small changes in cellular ROS. This mechanism may allow Rac1 to sense and regulate changes in cellular $O_2^{\bullet-}$ through SOD1 enzymatic conversion to H_2O_2. Such spatial regulation may be a key aspect of SOD1 function as a redox sensor and may explain the lack of therapeutic benefit from general ROS scavengers compared with direct inhibition of dysregulated Nox complexes with apocynin.

When considering the mechanism of the therapeutic effect of apocynin to inhibit Nox activation, it is worth noting several other potential aspects of this molecule that might also contribute to its neuroprotective effects in ALS mice. Apocynin can also inhibit other relevant enzymes that participate in cellular redox balance. For example, inhibition of Nox activity by apocynin has been linked to changes in the intracellular reduced/oxidized glutathione ratio and NF-κB–dependent cyclooxygenase-2 synthesis (35). Additionally, apocynin has been shown to alter the abundance of arachidonic acid–derived inflammatory mediators (36). Whether these apocynin-dependent effects are all linked to alterations in Nox activation remains to be fully investigated. There are also several factors that make apocynin appealing for clinical applications. Apocynin itself is inactive and only becomes active after the combined action of ROS and peroxidase activity (37). These characteristics theoretically minimize the off-target effects and makes the active metabolite largely available at sites of oxidative stress.

There are at least 2 key points worth considering about potential applications of apocynin to treat ALS in humans. First, it is unclear whether Nox dysregulation occurs in sporadic forms of ALS (not involving SOD1 mutations) that account for 90%–95% of cases. Second, it is also unclear at what point during the progression of ALS apocynin treatment could provide therapeutic benefit. To begin to address the latter question, we initiated apocynin treatment of ALS mice at 14, 60, and 80 days of age and evaluated survival (Supplemental Figure 5). In a relatively small cohort of sibling ALS mice, there was a significant benefit to treatment at all time points, although early intervention led to maximal therapeutic benefit. These findings suggest that inhibition of Nox activity during early phases of disease is important to slowing disease progression. Hence, early genetic diagnosis of patients with familial ALS would be critical for potential clinical applications with apocynin.

The appreciation that SOD1 is both a catabolic enzyme and regulatory protein involved in cellular ROS metabolism has potential broad-ranging implications for cell biology and the redox-dependent regulation of Rac1. The regulation of ROS production by Rac1 is important for many cellular processes involved in signal transduction (27), actin cytoskeletal rearrangements (28, 38, 39), and cell migration (29), proliferation (13, 29, 40, 41), and differentiation (30). In the context of redox-dependent signal transduction, it has become increasingly recognized that the localized production of $O_2^{\bullet-}$ and H_2O_2 at discrete subcellular domains appears to be a major regulatory aspect of pathways that depend on Nox-derived ROS (12, 42). Some of these pathways also involve activation and recruitment of Rac1 to specific membrane domains. Hence, further investigation into the role SOD1 plays in regulating the redox environment at discrete subcellular domains may uncover new layers of complexity in redox signaling in health, disease, and aging.

Methods

Cell culture and adenoviral infections

SH-SY and M059J cell lines were purchased from ATCC and cultured according to the manufacturer's instructions. Cells were infected with replication defected adenoviral vectors containing human WT or mutant SOD1 at 1,000 particles/cell when cells reached 70% confluency. Cells were harvested at 36, 48, and 72 hours after infection for Rac activation assays, Nox activity assays, and cell death assays, respectively. Recombinant adenoviruses expressing SOD1^{WT} or LacZ have been previously described (43). L8Q and G93A mutations in SOD1 were introduced into the pAd.CMVlinkwtSOD1 proviral vector using the Gene Editor in vitro site-directed mutagenesis system (Promega). Viruses were then generated as previously described (44).

Trypan blue exclusion assay

Cells were trypsinized and resuspended by gentle pipetting 72 hours after adenoviral infection. A 0.4% trypan blue solution (50 μl) was added to 200 μl cell suspension for a final trypan blue concentration of 0.08%. The cell suspension was then incubated for 2 minutes at room temperature, and the number of stained cells was counted using a hemocytometer. The percentage of dead cells was calculated as the number of stained cells divided by the total number of cells.

In situ DHE staining for $O_2^{\bullet-}$

Mice were euthanized with an overdose of sodium pentobarbital. The lumbar spinal cord was removed immediately and embedded in OTC as 4-mm-long segments. From each group, 30-μm sections were immediately gener-

ated within hours of embedding and stained in DHE as follows. Sections were rinsed in PBS containing 100 μM rotenone to inhibit mitochondrial respiration prior to incubation with 1 μM DHE (Invitrogen) for 5 minutes in the dark and the continued presence of 100 μM rotenone. Sections were then rinsed in PBS and coverslipped with Vectashield mounting media containing DAPI. DHE fluorescence was detected using a rhodamine emission filter. Microscope/camera exposure settings were kept constant between samples within an individual experiment, and control and experimental animals were always processed in parallel.

IP and Western blotting

SOD1-null mice (*Sod1*^{tm1Leb}) were purchased from Jackson Laboratories (45). Tissue lysates from WT and *SOD1* KO littermates were generated by homogenization in ice-cold PBS followed by the addition of an equal volume of 2× lysis buffer containing 40 mM Tris-HCl (pH 7.4), 300 mM NaCl, 2% Triton X-100, 100 mM NaF, 80 mM β-glycerophosphate, 10 mM EDTA, and a protease inhibitor cocktail tablet. Protein concentrations were measured by the Bradford assay. IP of Rac1 proteins was performed by incubating 600 μg total protein with 4 μg primary anti-Rac1 antibody (Upstate Cell Signaling Solutions) in 500 μl lysis buffer, followed by rotating for 2 hours at 4°C. Protein A-dynabeads, washed twice with lysis buffer, were then added and rotated overnight at 4°C, followed by magnetic removal of the IP complexes. Beads were washed 4 times with lysis buffer. Pellets were then resuspended in SDS-PAGE reducing loading buffer and incubated at 98°C for 5 minutes before separation by SDS-PAGE. The nitrocellulose membranes bearing the transferred proteins were blocked overnight at 4°C in blocking buffer containing 4% w/v nonfat dried milk and 0.3% Tween 20 in PBS and incubated with primary antibodies to SOD1 (The Binding Site Limited) and Rac1 (Santa Cruz Biotechnology Inc.) and then with infrared dye–conjugated secondary antibodies. Protein bands were detected by the Odyssey infrared imaging system (LI-COR Biotechnology).

Pulldown assays with His-tagged proteins

Dynabeads talon for His-tagged proteins were washed with potassium phosphate buffer (PPHB) containing 100 mM KH_2PO_4, 10 mM NaCl, 0.25 mM $MgCl_2$, and 100 nM $CaCl_2$. His-tagged Rac1 or Cdc42 (25 pmol) were incubated with 100 μl beads in PPHB at room temperature for 30 minutes with intermittent gentle agitation. The GTPases were either used directly or preloaded with 1 mM GTPγS or GDPβS in GTP binding buffer (50 mM HEPES (pH 7.6), 150 mM NaCl, and 0.1 mM EDTA) for 10 minutes at room temperature followed by the addition of $MgCl_2$ to 10 mM final concentration and wash in PPHB. Samples treated with H_2O_2 were resuspended in 1 ml PPHB containing the indicated H_2O_2 concentration for 30 minutes at room temperature and then washed 4 times with PPHB (1 ml each wash). SOD1 (250 pmol) in 10 μl PPHB was then added to each tube of beads, and samples were incubated at room temperature for 30 minutes with intermittent gentle agitation. Beads were then washed 3 times with PPHB to remove unbound SOD1. The fourth wash was carried out in 50 mM Tris (pH 6.8). Proteins were eluted using 20 μl 125 mM imidazole, and samples were then mixed with SDS-PAGE reducing loading buffer and separated by SDS-PAGE for Western blotting.

Rac1 GTPase assay

Rac1 GTPase assays were performed as previously described (46), with modifications. His-tagged Rac1 or Cdc42 (25 pmol) were incubated with 25 pmol GTP and 2.5 pmol P^{32}-labeled γ-GTP in GTP binding buffer containing 50 mM HEPES (pH 7.6), 150 mM NaCl, and 0.1 mM EDTA for 10 minutes at room temperature and then placed on ice water. A 1-μl aliquot was then taken for thin-layer chromatography (TLC) as time 0 of this GTPase reaction. Three proteins were added in various combinations to each reaction — including bovine SOD1, *E. coli* SOD1, and/or p29-GAP — as indicated in Results and figure legends. The molar ratio of Rac1 or Cdc42 to p29-GAP was 1:1. The molar ratio of Rac1 or Cdc42 to SOD1 was 1:10. To start the GTPase reaction, an equal volume of 2× GTPase buffer containing 50 mM HEPES (pH 7.6), 150 mM NaCl, 10 mM EDTA, and 10 mM $MgCl_2$ was added to each condition at 15°C. Where indicated, 100 mU xanthine oxidase was incubated in the reaction mixture with a final xanthine concentration of 100 μM. Aliquots (1 μl) were spotted on a TLC plate from each sample at different time points. The TLC was run for 90 minutes at room temperature in 1M acetic acid with 0.8M LiCl running buffer. To quantify GTP hydrolysis, the free phosphate (Pi) bands were cut out along with the corresponding GTP bands. Each was put in liquid scintillation fluid and counted by liquid scintillation spectrometry. The percentage of GTP hydrolyzed was calculated as Pi divided by the sum of Pi and GTP.

Construction of GST-Rac1 and GST-SOD1 fusion proteins

Bacterial expression constructs for WT and deletion mutants GST-Rac1 and/or GST-SOD1 were generated by PCR-mediated cloning into the pGex-2T vector (Amersham Biosciences). All bacterial fusion constructs were confirmed by complete sequencing. ALS mutations L8Q (47) and G10V (48) were introduced into the GST-SOD1 using the Gene Editor in vitro site-directed mutagenesis system (Promega). The primer sequence used to generate the L8Q mutant was 5′-AAGGCCGTGTGCGTGCAGAAGGGCGACGGCCCA-3′. The primer sequence used to generate the G10V mutant was 5′-AAGGCCGTGTGCGTGCTGAAGGTTGACGGCCCA-3′.

Expression and purification of bacterial GST-tagged proteins

The GST-tagged expression constructs were transformed into *E. coli* using ampicillin selection. Bacterial colonies harboring the WT and mutant constructs were grown in LB medium containing 100 μg/ml ampicillin in 1-l flasks at 37°C to a cell density of A_{600} = 0.6. Isopropyl-D-thiogalactopyranoside was then added to 1 mM to induce the expression of GST-tagged proteins, and cultures were grown for 6 hours at 37°C. The bacteria were collected by a 4,000 *g* spin for 15 minutes at 4°C and resuspended in PBS on ice. The bacteria were then lysed on ice by 5 30-seconds sonicator pulses using a virsonic cell disruptor (VirTis Gardiner). The bacterial lysate was then centrifuged at 30,000 *g* for 30 minutes to pellet debris. The fusion proteins were purified from cellular extracts using glutathione-sepharose beads (Amersham Biosciences) according to the manufacturer's instructions, and the GST fusion proteins were eluted with 10 mM glutathione, 50 mM Tris-HCl (pH 7.5), and 120 mM NaCl. Protein purity was assessed by Coomassie-stained SDS-PAGE, and protein concentrations were normalized using the Bradford method. It should be noted that GST-Rac1 fusion proteins containing 88 or 116 amino acids of the N terminus of Rac1 consistently migrated faster than their predicted molecular weights in SDS-PAGE, which was likely due to altered folding properties of domains contained within these deletion mutants. The GST-tagged SOD1 proteins were cleaved from GST using a thrombin cleavage capture kit (EMD Bioscences). Following cleavage, SOD1 proteins were separated from the cleaved GST-tag using an FPLC glutathione-sepharose column.

Demetalation of SOD1

Demetalation of purified bovine SOD1 was performed as previously described (1), with modification. Cu and Zn were removed by exposing purified bovine SOD1 to PBS (pH 3.0) plus 2 mM EDTA and stirring for 60 minutes at 4°C. The protein was then dialyzed overnight against 50 mM potassium phosphate (pH 7.4). A fraction of demetalated bovine SOD1 was then remetalated by dialysis against 100 mM sodium acetate (pH 5.5) in the presence of a 40-fold molar excess of Zn, followed by a 4-fold molar excess of Cu. To remove unbound metals, the SOD protein

was then dialyzed several times against PBS (pH 7.4). The Cu/Zn content of native, demetalated, and remetalated bovine SOD1 was determined as previously described (49). Briefly, 10 μg SOD1 was mixed with 1 ml assay buffer containing 100 mM sodium borate (pH 7.8), 2% SDS, and 100 μM pyridylazoresorcinol (PAR). The reaction mixture was heated for 20 minutes at 100°C. Zn and Cu levels were calculated as the decrease in 500-nm reading measured on a Shimadzu UV-160 spectrophotometer after the addition of 0.8 mM nitrilotriacetic acid (NTA) and EDTA, respectively. The Zn or Cu content in SOD1 was reported as the molar ratio of Zn or Cu to SOD1. SOD1 enzyme activity gels were performed as we described previously (43). Briefly, 10 μg native, demetalated, or remetalated SOD1 was run on a native 12% polyacrylamide gel. SOD1 activity was determined using nitroblue tetrazolium reduction. Enzymatic activity was defined as the clearance zones in a background of black precipitate.

Subcellular fractionation

Isolation of total endomembranes. Cells or tissue were lysed in homogenization buffer (50 mM Tris-HCl, 320 mM sucrose, and 1 mM EDTA, pH 7.4) by nitrogen cavitation. Lysate (600 μg) was then centrifuged at 3,000 *g* to create a postnuclear supernatant devoid of heavy mitochondria (PNS), and the supernatant was subsequently centrifuged at 100,000 *g* for 1 hour to spin down total endomembranes. The membranes were washed 3 times in homogenization buffer before being resuspended in 150 μl homogenization buffer prior to Nox activity assays.

Iodixanol separation of endosomes. Buoyant density centrifugation was used for subcellular fractionation and isolation of endosomes containing Nox2, Rac1, and SOD1 activity. Cells were washed twice with ice-cold PBS and scraped into a 1.5-ml microfuge tube using the same buffer. The cells were pelleted and resuspended in homogenization buffer (HMB) containing 0.25 M sucrose, 20 mM HEPES (pH 7.4), 1 mM EDTA, and an EDTA-free protease inhibitor cocktail. The cells were homogenized using nitrogen cavitation in a cell disruption high-pressure chamber (Parr instruments). The pressure was raised to 650 psi for 5 minutes and released suddenly. The homogenate was centrifuged at 3,000 *g* for 15 minutes to pellet unbroken cells, nuclei, and heavy mitochondria. The heavy mitochondrial supernatant (HMS) was bottom-loaded into an iodixanol discontinuous gradient in a 12.5-ml SW41Ti ultracentrifuge tube using a previously described method with modifications (50, 51). The discontinuous gradient was composed of 1.25 ml HMB without EDTA followed by bottom loading of the following sequential iodixanol steps: 1.0 ml 2.5%, 1.0 ml 5%, 1.5 ml 9%, 1.5 ml 14%, 2.5 ml 19%, 1.5 ml 26%, and finally the HMS in 2 ml 32%. Iodixanol concentrations were prepared fresh using a 50% iodixanol working solution (WS) diluted with HMB without EDTA. The WS was prepared by adding 1 part buffer containing 0.25 M sucrose and 120 mM HEPES (pH 7.4) to 5 parts iodixanol 60% stock solution. The gradients were centrifuged at 100,000 *g* using an SW41Ti swinging rotor overnight at 4°C. The fractions were collected from the top of the tube using a fraction collector (Labconco) in 500-μl fractions on ice. Endosomal fractions were concentrated by first diluting with buffer and centrifugation at 100,000 *g* for 1 hour, prior to Western blotting for various proteins. Fractions at the bottom of the gradient containing the sample loaded were not concentrated. The density gradient was designed to optimally separate the following compartments based on previous studies (51–55): fractions 1–5, plasma membrane (density, 1.03–1.05 g/ml); fractions 7–13, endosomal compartment (density, 1.055–1.11 g/ml); fractions 8–10, Golgi apparatus (density, 1.06–1.09 g/ml); fractions 10–13, light endoplasmic reticulum (density, 1.09–1.11 g/ml); fractions 13–18, lysozomes (density, 1.11–1.13 g/ml): fractions 18–21, light mitochondria (density, 1.13–1.15 g/ml); fractions 19–20, heavy endoplasmic reticulum (density, 1.145 g/ml); fractions 21–24, peroxisomes (density, 1.18–1.2 g/ml); and fractions 22–24, cytosolic proteins (density, 1.26 g/ml). Monoclonal antibody anti-Nox2 (54.1) was a kind gift from A.J. Jesaitis (Montana State University, Bozeman, Montana, USA; ref. 56) and W.M. Nauseef (University of Iowa).

Lucigenin chemiluminescence assay for NADPH-dependent $O_2^{\bullet-}$ production

Nox activities were analyzed by measuring the rate of $O_2^{\bullet-}$ generation using a chemiluminescent, lucigenin-based system (57). Lucigenin (5 μM) in 50 μl of each subcellular fraction (when iodixanol fractionation of PNS was used) or 100 μl of endomembranes (from 400 μg PNS) was incubated in the dark at room temperature for 15 minutes. Lucigenin chemiluminescence was measured using a single-tube Luminometer TD20-20 (Turner Designs). The reaction was initiated by the addition of β-NADPH to a final concentration of 100 μM with or without DPI (10 μM) and/or SOD (2.5 μM) as indicated. Lucigenin chemiluminescence was measured over the course of 5 minutes. The initial slope of the luminescence curve (RLU/min) was used to calculate the rate of luminescence product formation and compared between samples as an index of Nox activity. In the absence of NADPH, the luminescence was negligible and did not change over time.

Animal models

All animal experimentation met or exceeded the standards set by the principles and procedures outlined in the NIH guidelines for the care and use of experimental animals. All procedures were approved by the Animal Care and Use Committee at the University of Iowa. All mice were purchased from Jackson Laboratories. These included (a) *SOD1* KO mice (strain name, B6;129S7-*Sod1*$^{tm1Leb/J}$; stock no. 002972), (b) *Nox2* KO mice (strain name, B6.129S6$^{Cybbtm1Din/J}$; stock no. 002365), (c) transgenic mice overexpressing WT human *SOD1* [strain name, B6SJL-Tg(*SOD1*)$^{2Gur/J}$; stock no. 002297], control for transgenic mice overexpressing *SOD1*^{G93A}, and (d) transgenic mice overexpressing a human *SOD1*^{G93A} mutant transgene [strain name, B6SJL-Tg(SOD1G93A)$^{1Gur/J}$; stock no. 002726]. Genotypes were confirmed using PCR protocols given by Jackson Laboratories. Only transgenic mice hemizygous for the *SOD1*^{WT} or *SOD1*^{G93A} transgenes were used for analysis. The *SOD1*^{G93A} line of mice contains the high-expressing form of mutant SOD1, and animals develop disease onset at about 100 days of age and die about 25 days later (58). Clinical death was defined as the time when the mice could no longer right themselves within 20 seconds of being placed on their backs or when they lost 20% of their body weight during a 1-week period. If either of these 2 criteria was met, the mice were euthanized. At the time of advanced clinical symptoms, *SOD1*^{G93A} mice were grueled twice daily and individually housed.

Treatment of ALS mice with apocynin

Only mice hemizygous for the *SOD1*^{G93A} transgene were used in studies. Apocynin powder was added to hot (~60°C) sterile water at 3 different doses. The water was allowed to cool to room temperature before being given to the mice. The concentrations of apocynin tested were 200 μg/ml, 1 mg/ml, and 2 mg/ml in water. The conversion to mg/kg was estimated based on the average daily water intake of approximately 4 ml/mouse (which was confirmed in 25- to 30-g ALS mice; see also ref. 59), giving rise to dosing of approximately 30, 150, and 300 mg/kg/d. Water was changed every 5–7 days (a time point that demonstrated no detectable decay of apocynin by Electrospray LC-MS). Mice were started on apocynin-treated water at 14 days after birth unless otherwise indicated. The mice in the study were allowed free access to food and water. At the time of advanced clinical symptoms, mice were grueled twice daily with chow soaked in apocynin water or apocynin-free water. Those apocynin-treated *SOD1*^{G93A} transgenic mice that lived longer than untreated controls were susceptible to superficial eye infections. At first sign of discharge, mice were placed on water or gruel containing antibiotics (0.1 mg/ml gentamycin and 0.1 mg/ml ceftazidime). If the condition worsened,

mice were additionally injected subcutaneously with 85 mg/kg enterfloxin (Baytril) once daily for 14 days. To ensure that antibiotic treatment did not alter the course of ALS-like disease, *SOD1*^{G93A} transgenic mice were put on antibiotic water and monitored for survival (n = 8); no significant changes in survival were seen compared with untreated animals (data not shown).

Physiologic assays for disease

Beginning at 80 days of age, *SOD1*^{G93A} transgenic mice were evaluated for onset of motor neuron defects and disease symptoms by assessing both weight and stride length weekly. For stride length analysis, front and hind paws of mice were covered in different colored paint to record walking patterns during continuous locomotion. Stride length was measured, and the average stride was calculated from at least 6 consecutive strides (60).

Statistics

Statistical significance for all comparisons with the exception of survival curves was assessed using ANOVA followed by Dunnett's post-test or Student's t test. Kaplan-Meier survival curves were generated using Prism software and compared using the log-rank test; resulting P values are 2-tailed. In all statistical analyses, P values less than 0.05 were deemed significant.

Acknowledgments

This work was supported by the NIDDK (grant DK067928), the Roy J. Carver Chair in Molecular Medicine (J.F. Engelhardt), and the Center for Gene Therapy Animal Models Core (P30 DK54759). The authors would like to thank Jackie Bickenbach for help isolating the PMDFs. We also gratefully acknowledge Mariah Steele and Ola Awad for editorial assistance and Patricia Yarolem, Sara Nelson, and Andrea Park for technical assistance.

Received for publication September 26, 2007, and accepted in revised form November 28, 2007.

Address correspondence to: John F. Engelhardt, Room 1-111 BSB, Department of Anatomy and Cell Biology, Carver College of Medicine, University of Iowa, 51 Newton Road, Iowa City, Iowa 52242, USA. Phone: (319) 335-7744; Fax: (319) 335-6581; E-mail: john-engelhardt@uiowa.edu.

Maged M. Harraz and Jennifer J. Marden contributed equally to this work.

1. McCord, J.M., and Fridovich, I. 1969. Superoxide dismutase. An enzymic function for erythrocuprein (hemocuprein). *J. Biol. Chem.* **244**:6049–6055.
2. Rosen, D.R., et al. 1993. Mutations in Cu/Zn superoxide dismutase gene are associated with familial amyotrophic lateral sclerosis. *Nature.* **362**:59–62.
3. Wu, D.C., Re, D.B., Nagai, M., Ischiropoulos, H., and Przedborski, S. 2006. The inflammatory NADPH oxidase enzyme modulates motor neuron degeneration in amyotrophic lateral sclerosis mice. *Proc. Natl. Acad. Sci. U. S. A.* **103**:12132–12137.
4. Bruijn, L.I., Miller, T.M., and Cleveland, D.W. 2004. Unraveling the mechanisms involved in motor neuron degeneration in ALS. *Annu. Rev. Neurosci.* **27**:723–749.
5. Marden, J.J., et al. 2007. Redox modifier genes in amyotrophic lateral sclerosis in mice. *J. Clin. Invest.* **117**:2913–2919.
6. Boillee, S., et al. 2006. Onset and progression in inherited ALS determined by motor neurons and microglia. *Science.* **312**:1389–1392.
7. Lambeth, J.D. 2004. NOX enzymes and the biology of reactive oxygen. *Nat. Rev. Immunol.* **4**:181–189.
8. Hordijk, P.L. 2006. Regulation of NADPH oxidases: the role of Rac proteins. *Circ. Res.* **98**:453–462.
9. Furukawa, S., et al. 2004. Increased oxidative stress in obesity and its impact on metabolic syndrome. *J. Clin. Invest.* **114**:1752–1761.
10. Stolk, J., Hiltermann, T.J., Dijkman, J.H., and Verhoeven, A.J. 1994. Characteristics of the inhibition of NADPH oxidase activation in neutrophils by apocynin, a methoxy-substituted catechol. *Am. J. Respir. Cell Mol. Biol.* **11**:95–102.
11. Ueyama, T., Geiszt, M., and Leto, T.L. 2006. Involvement of Rac1 in activation of multicomponent Nox1- and Nox3-based NADPH oxidases. *Mol. Cell. Biol.* **26**:2160–2174.
12. Li, Q., et al. 2006. Nox2 and Rac1 regulate H2O2-dependent recruitment of TRAF6 to endosomal interleukin-1 receptor complexes. *Mol. Cell. Biol.* **26**:140–154.
13. Irani, K., et al. 1997. Mitogenic signaling mediated by oxidants in Ras-transformed fibroblasts. *Science.* **275**:1649–1652.
14. Abo, A., et al. 1991. Activation of the NADPH oxidase involves the small GTP-binding protein p21rac1. *Nature.* **353**:668–670.
15. Rae, T.D., Schmidt, P.J., Pufahl, R.A., Culotta, V.C., and O'Halloran, T.V. 1999. Undetectable intracellular free copper: the requirement of a copper chaperone for superoxide dismutase. *Science.* **284**:805–808.
16. Hirshberg, M., Stockley, R.W., Dodson, G., and Webb, M.R. 1997. The crystal structure of human rac1, a member of the rho-family complexed with a GTP analogue. *Nat. Struct. Biol.* **4**:147–152.
17. Ito, Y., et al. 1997. Regional polysterism in the GTP-bound form of the human c-Ha-Ras protein. *Biochemistry.* **36**:9109–9119.
18. Sprang, S.R. 1997. G protein mechanisms: insights from structural analysis. *Annu. Rev. Biochem.* **66**:639–678.
19. Worthylake, D.K., Rossman, K.L., and Sondek, J. 2000. Crystal structure of Rac1 in complex with the guanine nucleotide exchange region of Tiam1. *Nature.* **408**:682–688.
20. Rittinger, K., Walker, P.A., Eccleston, J.F., Smerdon, S.J., and Gamblin, S.J. 1997. Structure at 1.65 A of RhoA and its GTPase-activating protein in complex with a transition-state analogue. *Nature.* **389**:758–762.
21. Rittinger, K., et al. 1997. Crystal structure of a small G protein in complex with the GTPase-activating protein rhoGAP. *Nature.* **388**:693–697.
22. Menard, L., et al. 1992. Rac1, a low-molecular-mass GTP-binding-protein with high intrinsic GTPase activity and distinct biochemical properties. *Eur. J. Biochem.* **206**:537–546.
23. Roberts, A.W., et al. 1999. Deficiency of the hematopoietic cell-specific Rho family GTPase Rac2 is characterized by abnormalities in neutrophil function and host defense. *Immunity.* **10**:183–196.
24. Cheng, G., Diebold, B.A., Hughes, Y., and Lambeth, J.D. 2006. Nox1-dependent reactive oxygen generation is regulated by Rac1. *J. Biol. Chem.* **281**:17718–17726.
25. Zhao, X., Carnevale, K.A., and Cathcart, M.K. 2003. Human monocytes use Rac1, not Rac2, in the NADPH oxidase complex. *J. Biol. Chem.* **278**:40788–40792.
26. Wilkinson, B., Koenigsknecht-Talboo, J., Grommes, C., Lee, C.Y., and Landreth, G. 2006. Fibrillar beta-amyloid-stimulated intracellular signaling cascades require Vav for induction of respiratory burst and phagocytosis in monocytes and microglia. *J. Biol. Chem.* **281**:20842–20850.
27. Sulciner, D.J., et al. 1996. rac1 regulates a cytokine-stimulated, redox-dependent pathway necessary for NF-kappaB activation. *Mol. Cell. Biol.* **16**:7115–7121.
28. Kheradmand, F., Werner, E., Tremble, P., Symons, M., and Werb, Z. 1998. Role of Rac1 and oxygen radicals in collagenase-1 expression induced by cell shape change. *Science.* **280**:898–902.
29. Yamaoka-Tojo, M., et al. 2004. IQGAP1, a novel vascular endothelial growth factor receptor binding protein, is involved in reactive oxygen species-dependent endothelial migration and proliferation. *Circ. Res.* **95**:276–283.
30. Puceat, M., Travo, P., Quinn, M.T., and Fort, P. 2003. A dual role of the GTPase Rac in cardiac differentiation of stem cells. *Mol. Biol. Cell.* **14**:2781–2792.
31. Valentine, J.S., and Hart, P.J. 2003. Misfolded CuZnSOD and amyotrophic lateral sclerosis. *Proc. Natl. Acad. Sci. U. S. A.* **100**:3617–3622.
32. Barber, S.C., Mead, R.J., and Shaw, P.J. 2006. Oxidative stress in ALS: a mechanism of neurodegeneration and a therapeutic target. *Biochim. Biophys. Acta.* **1762**:1051–1067.
33. Galbussera, A., et al. 2006. Vitamin E intake and quality of life in amyotrophic lateral sclerosis patients: a follow-up case series study. *Neurol. Sci.* **27**:190–193.
34. Ferrante, K.L., et al. 2005. Tolerance of high-dose (3,000 mg/day) coenzyme Q10 in ALS. *Neurology.* **65**:1834–1836.
35. Barbieri, S.S., et al. 2004. Apocynin prevents cyclooxygenase 2 expression in human monocytes through NADPH oxidase and glutathione redox-dependent mechanisms. *Free Radic. Biol. Med.* **37**:156–165.
36. Engels, F., Renirie, B.F., Hart, B.A., Labadie, R.P., and Nijkamp, F.P. 1992. Effects of apocynin, a drug isolated from the roots of Picrorhiza kurroa, on arachidonic acid metabolism. *FEBS Lett.* **305**:254–256.
37. Hart, B.A., and Simons, J.M. 1992. Metabolic activation of phenols by stimulated neutrophils: a concept for a selective type of anti-inflammatory drug. *Biotechnol. Ther.* **3**:119–135.
38. Nimnual, A.S., Taylor, L.J., and Bar-Sagi, D. 2003. Redox-dependent downregulation of Rho by Rac. *Nat. Cell Biol.* **5**:236–241.
39. Lopes, N., et al. 2003. Thrombospondin 2 regulates cell proliferation induced by Rac1 redox-dependent signaling. *Mol. Cell. Biol.* **23**:5401–5408.
40. Pani, G., et al. 2000. A redox signaling mechanism for density-dependent inhibition of cell growth. *J. Biol. Chem.* **275**:38891–38899.
41. Moore, K.A., et al. 1997. Rac1 is required for cell proliferation and G2/M progression. *Biochem. J.* **326**:17–20.
42. Ushio-Fukai, M. 2006. Localizing NADPH oxidase-

derived ROS. *Sci. STKE.* **2006**:re8.
43. Zwacka, R.M., et al. 1998. Redox gene therapy for ischemia/reperfusion injury of the liver reduces AP1 and NF-kappaB activation. *Nat. Med.* **4**:698–704.
44. Anderson, R.D., Haskell, R.E., Xia, H., Roessler, B.J., and Davidson, B.L. 2000. A simple method for the rapid generation of recombinant adenovirus vectors. *Gene Ther.* **7**:1034–1038.
45. Matzuk, M.M., Dionne, L., Guo, Q., Kumar, T.R., and Lebovitz, R.M. 1998. Ovarian function in superoxide dismutase 1 and 2 knockout mice. *Endocrinology.* **139**:4008–4011.
46. Kwon, T., Kwon, D.Y., Chun, J., Kim, J.H., and Kang, S.S. 2000. Akt protein kinase inhibits Rac1-GTP binding through phosphorylation at serine 71 of Rac1. *J. Biol. Chem.* **275**:423–428.
47. Bereznai, B., Winkler, A., Borasio, G.D., and Gasser, T. 1997. A novel SOD1 mutation in an Austrian family with amyotrophic lateral sclerosis. *Neuromuscul. Disord.* **7**:113–116.
48. Kim, N.H., Kim, H.J., Kim, M., and Lee, K.W. 2003. A novel SOD1 gene mutation in a Korean family with amyotrophic lateral sclerosis. *J. Neurol. Sci.* **206**:65–69.
49. Ghezzo-Schoneich, E., Esch, S.W., Sharov, V.S., and Schoneich, C. 2001. Biological aging does not lead to the accumulation of oxidized Cu,Zn-superoxide dismutase in the liver of F344 rats. *Free Radic. Biol. Med.* **30**:858–864.
50. Xia, W., et al. 1998. Presenilin 1 regulates the processing of beta-amyloid precursor protein C-terminal fragments and the generation of amyloid beta-protein in endoplasmic reticulum and Golgi. *Biochemistry.* **37**:16465–16471.
51. Graham, J., Ford, T., and Rickwood, D. 1994. The preparation of subcellular organelles from mouse liver in self-generated gradients of iodixanol. *Anal. Biochem.* **220**:367–373.
52. Billington, D., Maltby, P.J., Jackson, A.P., and Graham, J.M. 1998. Dissection of hepatic receptor-mediated endocytic pathways using self-generated gradients of iodixanol (Optiprep). *Anal. Biochem.* **258**:251–258.
53. Graham, J.M., and Billington, D. 1996. Iodixanol — a new density gradient medium for the dissection of the endosomal compartment. *Z. Gastroenterol.* **34**(Suppl. 3):76–78.
54. Graham, J.M. 2002. Purification of peroxisomes using a density barrier in a swinging-bucket rotor. *ScientificWorldJournal.* **2**:1400–1403.
55. Plonne, D., et al. 1999. Separation of the intracellular secretory compartment of rat liver and isolated rat hepatocytes in a single step using self-generating gradients of iodixanol. *Anal. Biochem.* **276**:88–96.
56. Burritt, J.B., Quinn, M.T., Jutila, M.A., Bond, C.W., and Jesaitis, A.J. 1995. Topological mapping of neutrophil cytochrome b epitopes with phage-display libraries. *J. Biol. Chem.* **270**:16974–16980.
57. Li, Y., et al. 1998. Validation of lucigenin (bis-N-methylacridinium) as a chemilumigenic probe for detecting superoxide anion radical production by enzymatic and cellular systems. *J. Biol. Chem.* **273**:2015–2023.
58. Gurney, M.E., et al. 1994. Motor neuron degeneration in mice that express a human Cu,Zn superoxide dismutase mutation. *Science.* **264**:1772–1775.
59. Bachmanov, A.A., Reed, D.R., Beauchamp, G.K., and Tordoff, M.G. 2002. Food intake, water intake, and drinking spout side preference of 28 mouse strains. *Behav Genet* **32**:435–443.
60. Harper, S.Q., et al. 2005. RNA interference improves motor and neuropathological abnormalities in a Huntington's disease mouse model. *Proc. Natl. Acad. Sci. U. S. A.* **102**:5820–5825.